ACS APPLIED MATERIALS & INTERFACES

www.acsami.org Research Article

Controlling Anti-Penetration Performance by Post-Grafting of Fluorinated Alkyl Chains onto Polystyrene-*block*-poly(vinyl methyl siloxane)

Zhenglin Zhang, Krishnaroop Chaudhuri, Florian Kaefer, Anthony P. Malanoski, Kirt A. Page, Louisa M. Smieska, Jonathan T. Pham, and Christopher K. Ober*

Cite This: https://doi.org/10.1021/acsami.4c01905 Read Online

ACCESS | Metrics & More | Article Recommendations | Supporting Information

ABSTRACT: Polydimethylsiloxane (PDMS) has been widely used as a surface coating material, which has been reported to possess dynamic omniphobicity to a wide range of both polar and nonpolar solvents due to its high segmental flexibility and mobility. However, such high flexibility and mobility also enable penetration of small molecules into PDMS coatings, which alter the chemical and physical properties of the coating layers. To improve the anti-penetration properties of PDMS, a series of fluorinated alkyl segments are grafted to a diblock copolymer of polystyrene-*block*-poly(vinyl methyl siloxane) (PS-*b*-PVMS) using thiol−ene click reactions. This article reports the chemical characterization of these model fluorosilicone block copolymers and uses fluorescence measurements to investigate the dye penetration characteristics of polymer thin films. The introduction of longer fluorinated alkyl chains can gradually increase the anti-penetration properties as the time to reach the maximum fluorescence intensity (t_{peak}) gradually increases from 11 s of PS-*b*-PVMS to more than 1000 s of PS-*b*-P(*n*-C_6F_{13}-VMS). The improvement of anti-penetration properties is attributed to stronger inter-/intrachain interactions, phase segregation of ordered fluorinated side chains, and enhanced hydrophobicity caused by the grafting of fluorinated alkyl chains.

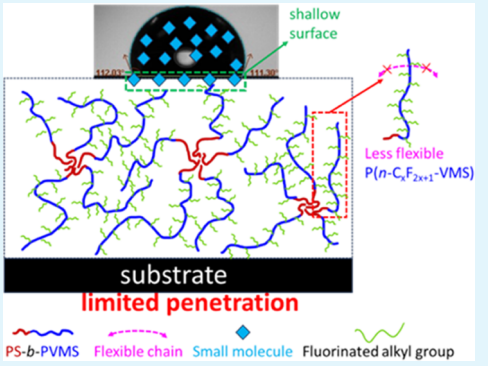

KEYWORDS: *polydimethylsiloxane, coating, antipenetration, fluorination, in situ fluorescence*

INTRODUCTION

Control of penetration, the phenomenon of small molecules passing through a polymer layer, is highly desired in many applications, such as anticorrosion of metal substrates,[1] anti-graffiti coatings,[2] wastewater treatment,[3] and gas separation.[4] In addition to these uses, polydimethylsiloxane (PDMS) is widely employed as a surface coating material for anti-fouling,[5] anti-protein,[6] anti-friction,[7] anti-icing,[8] and self-cleaning applications[9−11] due to its low surface energy of 20.4 mN/m[12] and the ability of PDMS coatings to covalently bond to a broad range of substrates.[13−16] The penetration of small molecules, such as solvent molecules, in PDMS materials is common and occurs in microfluid devices,[17,18] membranes,[19,20] and sensors,[21,22] which is known to lead to swelling of PDMS in some cases[23] and produce changes to its chemical and physical properties.[21,22,24−28] Furthermore, the liquid-like behavior of PDMS (due to its low rotation barrier around the Si−O bond (3.3 kcal/mol), weak inter-/intrachain interactions, and the low glass transition temperature of PDMS (−127 °C))[12] not only results in dynamic omniphobicity (a surface property repelling both polar and nonpolar solvents and allowing liquid droplets to roll off easily at small tilting angles) on its brush-type coatings[29,30] but can also enhance the ability of small molecules to penetrate a PDMS layer.[31] Especially for coatings that are immersed in a penetrant for extended times, such as barrier materials or even hull marine antifouling coatings, the time-dependent penetration of unwanted small molecules may also be a key consideration in the selection of coating materials. For example, the hydrolysis of PDMS coatings during water penetration may reduce their durability and hydrophobicity after immersion in water for extended periods.[8] Recently, the permeation of NaCl and $CaCl_2$ salts through a PDMS membrane and their deposition on its substrate has also been reported,[32] which will compromise the application of a PDMS coating system for anticorrosion in high-salinity seawater.

To control penetration in PDMS coatings, methods have been developed using crosslinking to limit PDMS chain flexibility and mobility[31,33−35] or using coatings to form

Received: February 1, 2024
Revised: March 24, 2024
Accepted: March 28, 2024

Scheme 1. Synthesis Routes of (a) *n*-$C_xF_{2x+1}(CH_2)_2SH$ and (b) PS-*b*-P(*n*-C_xF_{2x+1}-VMS)

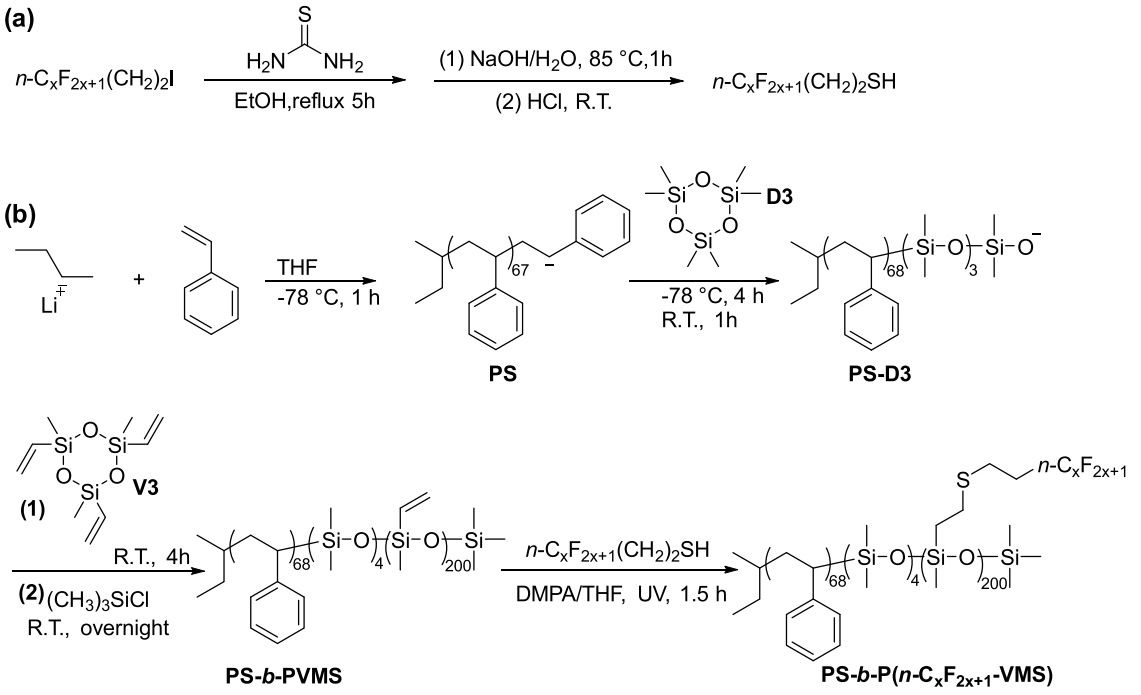

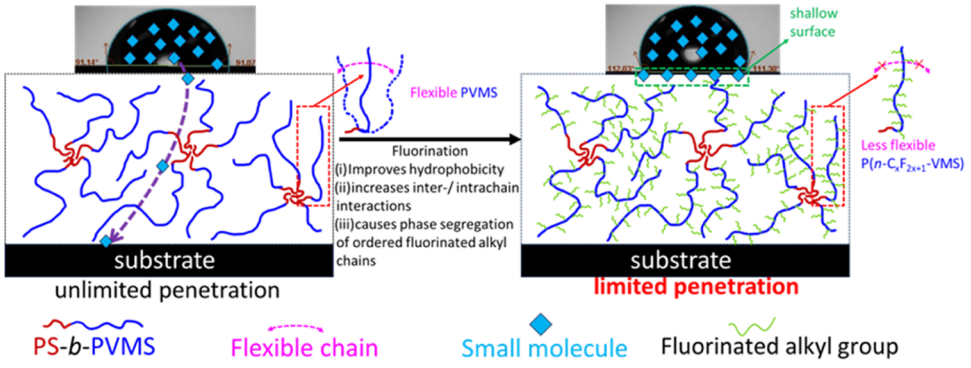

Figure 1. Fluorination of PS-*b*-PVMS polymers to provide better anti-penetration performances through improved hydrophobicity, stronger inter-/intrachain interactions, and phase segregation.

additional protective films to prevent access to the PDMS layer.[36−38] However, these methods cannot guarantee that all flexible segments are fixed in the cross-linked networks. The coatings may also require complicated processes for additional protective layers, including vapor deposition, plasma oxidation, and further surface reactions. Compared with the above methods, introducing specific functional groups onto PDMS can directly tailor the physical and chemical properties.[39,40] For example, PDMS functionalized with poly(ethylene glycol) methyl ether acrylate can improve the permeability of CO_2 and selectivity over N_2.[40]

Block polymers of PS-*b*-PDMS were specifically designed for antifouling applications in our previous research, where the PS block can act as an anchor in a pretreated surface coated with polystyrene-*block*-poly(ethylene-*ran*-butylene)-*block*-polystyrene to physically hold the PS-*b*-PDMS.[41] And our recent antipenetration paper on block copolymers of PS-*b*-PDMS indicated that a higher weight fraction of PDMS would reduce surface coatings' anti-penetration properties.[42] In this paper, we present an easy and effective method to directly functionalize PDMS with a series of fluorinated alkyl chains by thiol−ene click reactions[41] to gradually tune its material properties and study anti-penetration behavior. The addition of fluorinated alkyl chains to PDMS is expected to improve its anti-penetration properties because of the hydrophobicity and oleophobicity of fluorinated alkyl chains, which can suppress wetting by solvents and subsequent penetration.[2] However, the influence of the length of fluorinated alkyl groups on the anti-penetration properties of PDMS has not been explored in a systematic manner. Here, through the thiol−ene click reactions on the vinyl groups of polystyrene-*block*-poly(vinyl methyl siloxane) (PS-*b*-PVMS) with fluorinated alkyl thiols (*n*-$C_xF_{2x+1}(CH_2)_2SH$) (x = 1−4, 6), we synthesized a series of fluorosilicone block copolymers (PS-*b*-P(*n*-C_xF_{2x+1}-VMS), see Scheme 1). The resulting polymers were characterized by nuclear magnetic resonance (NMR) spectroscopy, differential scanning calorimetry (DSC), small-angle X-ray scattering (SAXS), and water contact angle measurements to reveal the effect of fluorination on the polymer flexibility, mobility, and hydrophobicity, while anti-penetration behaviors are observed by an in situ confocal microscopy method. Our results show that fluorination not only improves coating hydrophobicity but

https://doi.org/10.1021/acsami.4c01905
ACS Appl. Mater. Interfaces XXXX, XXX, XXX−XXX

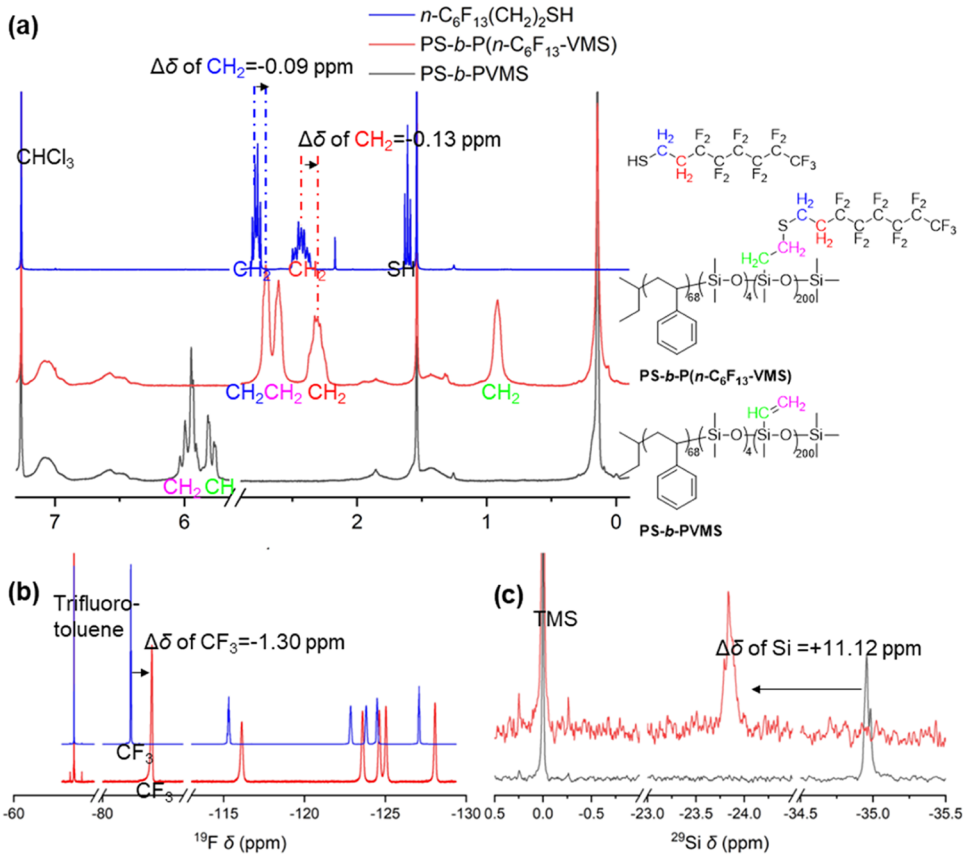

Figure 2. ^{1}H NMR (a), ^{19}F NMR (b), and ^{29}Si NMR spectra (c) for n-$C_6F_{13}(CH_2)_2SH$, PS-b-PVMS, and PS-b-P(n-C_6F_{13}-VMS) in $CDCl_3$. The "+" and "−" are generated from the difference in chemical shifts ($\Delta\delta$) between PS-b-P(n-C_6F_{13}-VMS) and n-$C_6F_{13}(CH_2)_2SH$ or PS-b-PVMS, which indicate that the chemical shifts of PS-b-P(n-C_6F_{13}-VMS) move downfield and upfield, respectively.

also increases intra- and interchain interactions and causes phase segregation of ordered fluorinated side chains, which can limit the flexibility and mobility of the PDMS backbone and improve anti-penetration proporties (see Figure 1).

RESULTS AND DISCUSSION

A diblock copolymer PS-b-PVMS ($\bar{M}_n$ of PS = 7.2 kg/mol based on GPC, $\bar{M}_n$ of PVMS = 17.2 kg/mol based on NMR, dispersity ($Đ$) = 1.2, see Table S1 and Figure S1) was synthesized by a sequential anionic polymerization, which was further functionalized by thiol−ene click reactions with n-$C_xF_{2x+1}(CH_2)_2SH$ (see Scheme 1). Details of the synthesis and characterization of fluorinated thiols, PS-b-PVMS, and PS-b-P(n-C_xF_{2x+1}-VMS) can be found in the Experimental Section. NMR spectra in Figure 2 show that n-$C_6F_{13}(CH_2)_2SH$ was successfully grafted to PS-b-PVMS—the signals of the vinyl group of PS-b-PVMS (the multiplets between 5.70 and 6.20 ppm) and the signals of the thiol group of n-$C_6F_{13}(CH_2)_2SH$ (the triplet at 1.61 ppm) were not observed in the ^{1}H NMR spectrum of PS-b-P(n-C_6F_{13}-VMS). Instead, four methylene groups (labeled with green, pink, blue, and red) with a ratio of integration areas of 1:1:1:1 can be detected in the ^{1}H NMR spectrum of PS-b-(n-C_6F_{13}-PVMS). At the same time, the ^{29}Si NMR spectrum shifted from −34.96 to −23.84 ppm, which indicates that all vinyl groups were converted to methylene groups.[43] For the ^{19}F NMR spectrum of PS-b-P(n-C_6F_{13}-VMS) (see Figure 2b), similar fluorine chemical shifts can be detected as in n-$C_6F_{13}(CH_2)_2SH$, but all fluorine signals shifted upfield compared with corresponding fluorine signals from n-$C_6F_{13}(CH_2)_2SH$. For example, the chemical shift of CF_3 in PS-b-P(n-C_6F_{13}-VMS) shifted upfield with a difference of chemical shift ($\Delta\delta$) of −1.30 ppm relative to the CF_3 in n-$C_6F_{13}(CH_2)_2SH$. Upfield shifting can also be observed for the two methylene groups of the fluorinated alkyl chain (labeled with blue and red), indicating that the fluorinated alkyl chain was shielded by higher electron density after the thiol−ene reaction. The upfield shifting in ^{1}H and ^{19}F NMR spectra of the n-$C_xF_{2x+1}(CH_2)_2$ group increases with a longer fluorinated alkyl chain (see Table 1). While using PS-b-PVMS as a reference, an increased downfield shift can be observed in the

Table 1. Difference of Chemical Shifts ($\Delta\delta$) of PS-b-P(n-C_xF_{2x+1}-VMS) Compared to n-$C_xF_{2x+1}(CH_2)_2SH$ (^{1}H and ^{19}F NMR) and PS-b-PVMS (^{29}Si NMR)

polymer	$\Delta\delta$ in ^{1}H NMR[a] (ppm)	$\Delta\delta$ in ^{19}F NMR[b] (ppm)	$\Delta\delta$ in ^{29}Si NMR[c] (ppm)
PS-b-P(CF_3-VMS)	−0.02, −0.05	−0.13	+11.08
PS-b-P(n-C_2F_5-VMS)	−0.02, −0.07	−0.17	+11.09
PS-b-P(n-C_3F_7-VMS)	−0.03, −0.09	−0.35	+11.09
PS-b-P(n-C_4F_9-VMS)	−0.06, −0.09	−0.59	+11.10
PS-b-P(n-C_6F_{13}-VMS)	−0.09, −0.13	−1.30	+11.12

[a]The $\Delta\delta$ of ^{1}H NMR between the corresponding methylene groups (marked as blue, left in the column, and red, right in the column, in Figure 2) in PS-b-P(n-C_xF_{2x+1}-VMS) and n-$C_xF_{2x+1}(CH_2)_2SH$. [b]The $\Delta\delta$ of^{19}F NMR between the terminal CF_3 groups in PS-b-P(n-C_xF_{2x+1}-VMS) and n-$C_xF_{2x+1}(CH_2)_2SH$. [c]The $\Delta\delta$ of ^{29}Si NMR between PS-b-P(n-C_xF_{2x+1}-VMS) and PS-b-PVMS.

https://doi.org/10.1021/acsami.4c01905
ACS Appl. Mater. Interfaces XXXX, XXX, XXX−XXX

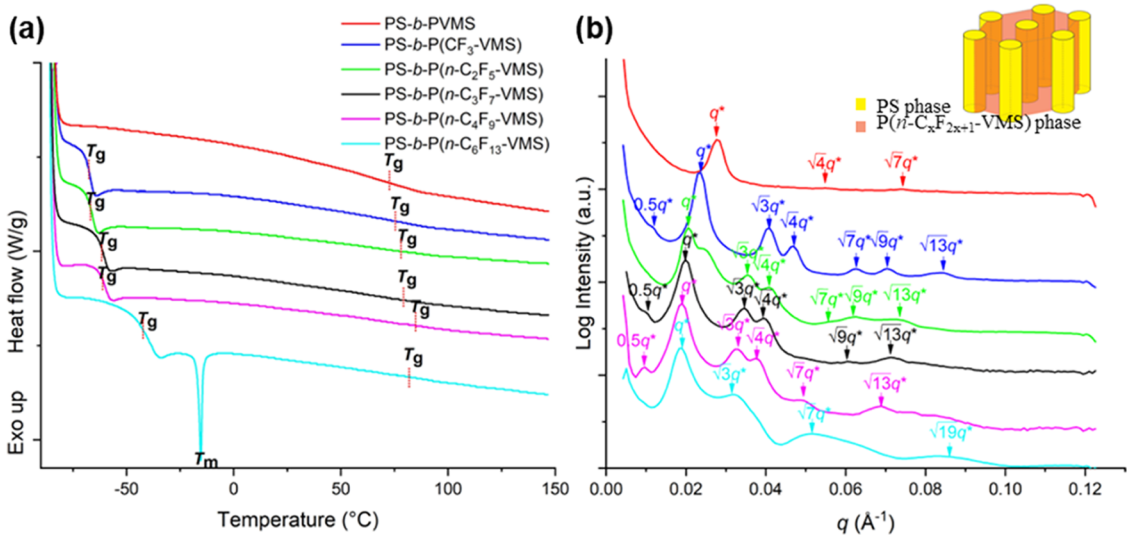

Figure 3. (a) DSC thermograms of PS-*b*-P(*n*-C_xF_{2x+1}-VMS) measured on the second heating scan at 10 °C/min. (b) SAXS profiles of PS-*b*-P(*n*-C_xF_{2x+1}-VMS) and a hypothesized model of hexagonally packed cylinders, where q^* is the primary peak for each SAXS profile and all peaks are marked with colorful arrows and relative values of q^*. Note: the same color system is used in parts (a) and (b) to represent the tested polymers.

Table 2. Measured Glass Transition Temperatures of PS-*b*-P(*n*-C_xF_{2x+1}-VMS) and Previously Reported Glass Transition Temperatures of Poly(alkylmethylsiloxane)

polymers reported in this paper	T_g of PVMS block (°C)	T_g of PS block (°C)	polymers reported before[53]	T_g (°C)
PS-*b*-PVMS	[a]	73	PDMS	−126
PS-*b*-P(CF_3-VMS)	−68	75	poly(ethylmethylsiloxane)	−139
PS-*b*-P(*n*-C_2F_5-VMS)	−67	78	poly(*n*-propylmethylsiloxane)	−120
PS-*b*-P(*n*-C_3F_7-VMS)	−62	79	poly(*n*-butylmethylsiloxane)	−115
PS-*b*-P(*n*-C_4F_9-VMS)	−61	85	poly(*n*-pentylmethylsiloxane)	−112
PS-*b*-P(*n*-C_6F_{13}-VMS)	−42	82	poly(*n*-hexylmethylsiloxane)	−108

[a]The T_g of PVMS was reported to be around −100 °C.[48]

Table 3. Composition, SAXS Morphology Data, and Water Contact Angle of PS-*b*-P(*n*-C_xF_{2x+1}-VMS)

polymer	polymer's molar mass	weight fraction of *n*-C_xF_{2x+1}	weight fraction of PS	q^*(Å^{-1})	$d_{spacing}$ (nm)	water contact angle (deg)
PS-*b*-PVMS	24 743	0	29%	0.028	23	91.9 ± 0.9
PS-*b*-P(CF_3-VMS)	50 769	27%	14%	0.024	26	85.1 ± 2.3
PS-*b*-P(*n*-C_2F_5-VMS)	60 771	39%	11%	0.021	30	98.7 ± 1.0
PS-*b*-P(*n*-C_3F_7-VMS)	70 771	48%	10%	0.020	32	106.7 ± 0.9
PS-*b*-P(*n*-C_4F_9-VMS)	80 733	54%	9%	0.019	33	110.2 ± 1.0
PS-*b*-P(*n*-C_6F_{13}-VMS)	100 777	63%	7%	0.019	33	111.2 ± 2.0

^{29}Si NMR spectra of PS-*b*-P(*n*-C_xF_{2x+1}-VMS) (Table 1 and Figure S6). Therefore, the NMR results imply interactions between silicon and fluorine in PS-*b*-P(*n*-C_6F_{13}-VMS) as the electron donor and electron acceptor, respectively. Such interactions between silicon and fluorine were also reported in polysilanes.[44,45] The degree of chemical shifts mentioned above increases with the length of fluorinated alkyl chains, which implies that a longer fluorinated alkyl chain can result in stronger inter- and intrachain interactions because of the attraction between the atoms of fluorine and silicon.

The thermal properties of the fluorinated PS-*b*-PVMS polymers were characterized by DSC. A first heating cycle during DSC runs was employed to remove any prior thermal history, and DSC thermograms of the second heating cycle are shown in Figure 3a; the related T_gs can be found in Table 2. Two glass transition temperatures for both PS and PVMS blocks would be expected due to phase separation of PS and polysiloxane.[46,47] For the synthesized PS-*b*-PVMS, a T_g of 73 °C for the PS block was detected, while the T_g of the PVMS block was not detected as it is about −100 °C[48] and out of the tested range. After grafting fluorinated alkyl chains onto PS-*b*-PVMS, the T_g increases with the length of the fluorinated alkyl chain from −68 to −42 °C. For PS-*b*-P(*n*-C_6F_{13}-VMS), a melting signal at around −15 °C is observed with an enthalpy of 1.32 J/g, which may be the result of melting ordered domains formed by the longer side chain of *n*-C_6F_{13}.[49−52] A similar T_g trend was also reported in polymers of poly(*n*-alkylmethylsiloxane), where the T_g increased from −126 to −108 °C when the length of the *n*-alkyl group increased from a methyl group to an *n*-hexyl group (see Table 2).[53] Both fluorinated alkyl chains and nonfluorinated alkyl chains can increase the T_g of polysiloxanes, but the fluorinated ones show a stronger influence. This is evident by comparing the T_g of −68 °C in PS-*b*-P(CF_3-VMS) and the T_g of −108 °C in poly(*n*-hexylmethylsiloxane), where they have a similar side chain length. The increase in T_g of PVMS was observed with

https://doi.org/10.1021/acsami.4c01905
ACS Appl. Mater. Interfaces XXXX, XXX, XXX−XXX

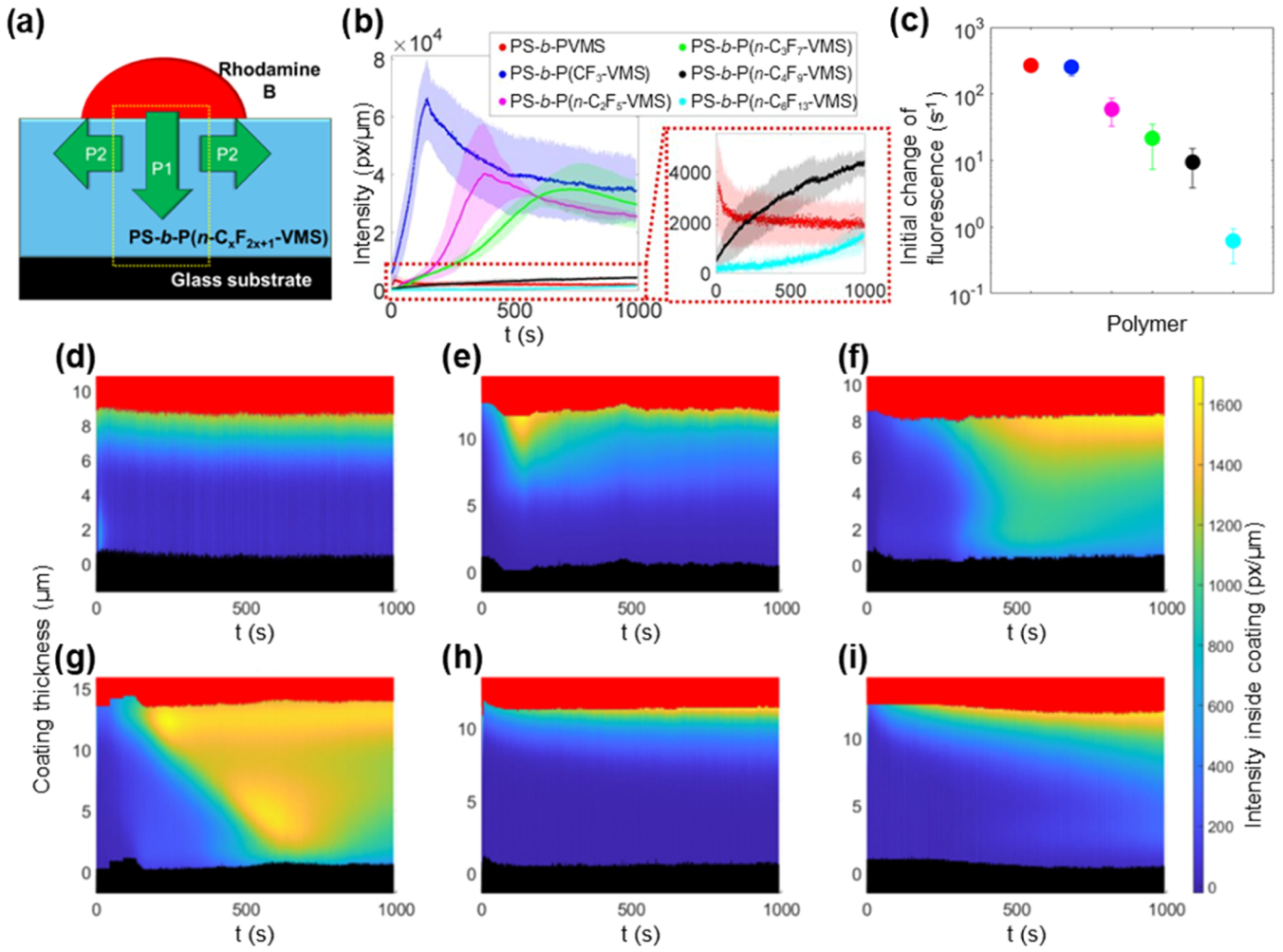

Figure 4. (a) Schematic (not to scale) of the imaging setup for penetration experiments. The yellow dashed box represents the area under observation by a confocal microscope, which is imaged from the bottom. P1 and P2 denote dye penetration occurring in the downward and lateral directions, respectively. (b) Total fluorescence intensity in coatings of different PS-*b*-P(*n*-C_xF_{2x+1}-VMS) species vs time. For clarity, the species where x = 0, 4, and 6 have been plotted separately (red dotted box). Shaded areas represent errors calculated by taking the standard deviation over three experiments. The spatiotemporal fluorescence intensities of PS-*b*-PVMS(d), PS-*b*-P(CF_3-VMS) (e), PS-*b*-P(*n*-C_2F_5-VMS) (f), PS-*b*-P(*n*-C_3F_7-VMS) (g), PS-*b*-P(*n*-C_4F_9-VMS) (h), and PS-*b*-P(*n*-C_6F_{13}-VMS) (i) in the test area were recorded to track the dye penetration behavior over both coating thickness (vertical axis) and time (horizontal axis), where the color inside the coating layer represents the z-axis fluorescence intensity (the color bar). The fluorescence intensities in part (b) have been calculated by integrating the spatiotemporal fluorescence intensities (over the vertical axis) in the coating region. The drop and the glass regions have been excluded from the calculations and are artificially colored red and black for clarity, respectively. (c) Rate of change in fluorescence intensity in the coatings just after the deposition of the drops. The values are calculated by measuring the slope of a straight line (d[fluorescence intensity]/dt) that best fits the data in part (b) for time scales much less than the peak formation time. Errors are calculated from the standard deviation over 3 samples. Note: the same color system is used in parts (b) and (c) to represent the tested polymers.

the length of the fluorinated alkyl chain, which implies that the flexibility of PVMS was limited by a longer fluorinated alkyl chain. Decreasing chain flexibility and enabling fluorinated domain formation may be beneficial for limiting small molecular penetration. For T_g of the PS block, it became less obvious after fluorination, which can be attributed to the decreased mass percentage of the PS block (from 29 to 7%, see Table 3) and the small change in the heat capacity of the PS block near its T_g.[46]

The grafting of fluorinated alkyl chains on PS-*b*-PVMS also decreased their solubility in THF as shown in Figure S7. For PS-*b*-PVMS and PS-*b*-P(*n*-C_xF_{2x+1}-VMS) with x = 1 and 2, they dissolved well in THF (concentration = 80 mg/mL), and the solution flowed after inverting the vials. However, for PS-*b*-P(*n*-C_xF_{2x+1}-VMS) with x = 3, 4, and 6, their solutions cannot flow at the same concentration and stick on the bottom of the vials. These phenomena also support the fact that PS-*b*-P(*n*-C_xF_{2x+1}-VMS) with longer fluorinated alkyl chains has stronger cohesion among polymer chains.

The effect of fluorination on the morphology of bulk samples of PS-*b*-P(*n*-C_xF_{2x+1}-VMS) was investigated by SAXS. The morphologies of PS-*b*-PDMS polymers have been widely explored due to the phase separation between PS and PDMS. Factors such as weight fractions of PS and PDMS,[46,54] solvents' selectivity,[55] plasticizers,[56] and topologies of block polymers of PS and PDMS were reported to significantly affect the morphology.[57,58] For this study, we focus on the influence of the fluorinated alkyl chain length on the morphology of PS-*b*-PVMS. As shown in Figure 3b, the SAXS profile of PS-*b*-PVMS shows that its morphology matches that of hexagonally packed

https://doi.org/10.1021/acsami.4c01905
ACS Appl. Mater. Interfaces XXXX, XXX, XXX−XXX

cylinders (HEX) as the relative values of q/q^* are 1, $\sqrt{4}$, and $\sqrt{7}$, which are the (1,0), (2,0), and (2,1) peaks of the hexagonal lattice, respectively.[59] For PS-*b*-P(CF_3-VMS), its SAXS profile shows more peaks with q/q^* of 1, $\sqrt{3}$, $\sqrt{4}$, $\sqrt{7}$, $\sqrt{9}$, and $\sqrt{13}$, which are the (1,0), (1,1), (2,0), (2,1), (3,0), and (3,1) peaks of a HEX, respectively.[60] Compared with PS-*b*-PVMS, the SAXS results show that PS-*b*-P(CF_3-VMS) has a morphology of more ordered HEX, which may be explained by the limitation of the flexibility of the PVMS backbone after the introduction of CF_3 that can limit the deformation of its microdomain.[61] For the SAXS data of PS-*b*-P(n-C_xF_{2x+1}-VMS) with x = 2−4, most of the characteristic peaks of HEX can be observed as in PS-*b*-P(CF_3-VMS); we can also notice one new shoulder peak between q^* and $\sqrt{3}q^*$ for PS-*b*-P(n-C_2F_5-VMS), disappearance of the peak at $\sqrt{7}q^*$ for PS-*b*-P(n-C_3F_7-VMS), and disappearance of the peak at $\sqrt{9}q^*$ for PS-*b*-P(n-C_4F_9-VMS). A small peak of $0.5q^*$ can be found in the SAXS profiles of PS-*b*-P(n-C_xF_{2x+1}-VMS) when x = 1, 3, and 4, which may be from a long-order structure.[62] Furthermore, only peaks of q^*, $\sqrt{3}q^*$,$\sqrt{7}q^*$, and $\sqrt{19}q^*$ (from (3,2) of a HEX) can be observed for PS-*b*-P(n-C_6F_{13}-VMS). The change of SAXS pattern from HEX of PS-*b*-P(CF_3-VMS) becomes more obvious with a longer fluorinated alkyl chain and may be explained by the decreased weight fraction of PS (see Table 3) and phase segregation of ordered fluorinated side chains. Especially for PS-*b*-P(n-C_6F_{13}-VMS), the crystallization caused by the n-C_6F_{13} side chain, as indicated by the melting signal in DSC, may further prevent the formation of a classic HEX morphology. On the other hand, both PS-*b*-P(n-C_6F_{13}-VMS) and PS-*b*-P(n-C_4F_9-VMS) have the same $d_{spacing}$ of 33 nm, and the peaks at $q^*$and $\sqrt{3}q^*$of PS-*b*-P(n-C_6F_{13}-VMS) are wider than the corresponding peaks of PS-*b*-P(n-C_4F_9-VMS). These may indicate that tighter packing structures with a broader distribution of the distances between adjacent PS cylinders existed in PS-*b*-P(n-C_6F_{13}-VMS), which may be caused by the crystallization. In addition to the weak interactions of fluorinated alkyl chains with guest molecules because of its low polarizability,[63] a tighter packing would help the formation of fluorinated domains and hinder small molecule transport, which would be beneficial for creating protective barrier coatings.

To study the surface wetting properties after fluorination, water contact angles of PS-*b*-P(n-C_6F_{13}-VMS) were measured by a standard, static sessile drop method. The average water contact angle decreased from 92° of PS-*b*-PVMS to 85° of PS-*b*-P(CF_3-VMS) and then kept increasing with the length of the fluorinated alkyl chain until it reached 111° for PS-P(n-C_6F_{13}-VMS) (see Table 3). The decrease of the water contact angle of PS-*b*-P(CF_3-VMS) can be explained by a strong dipole caused by the group of CH_2CF_3, which would increase the dipole−dipole interactions with water and result in a higher wettability.[64,65] For longer fluorinated alkyl chains, the CH_2CF_2 group would be buried by the n-$C_{x-1}F_{2x-1}$ group and stay away from the surface; therefore, the hydrophobicity caused by the fluorinated alkyl chain would dominate the surface properties and show higher water contact angle.[66,67]

The penetration behavior of a fluorescent dye into PS-*b*-P(n-C_xF_{2x+1}-VMS) was measured by recording the spatiotemporal change in fluorescence inside the coating using in situ confocal microscopy after a dye-loaded aqueous solution drop was placed on the target layer (Figure 4a). Rhodamine B was used as a model penetrant since it penetrates neat PDMS and can be tracked fluorescently. A more detailed setup and description of the penetration experiment can be found in the Experimental Section and in our previous publication.[42] The fluorescence intensity distribution in the coating is shown for the polymers with different fluorinations (Figure 4d−i).To obtain a more intuitive understanding of the change in penetration kinetics, the intensity inside the coating is integrated along the spatial vertical axis to obtain the total change in fluorescence inside the coating over time (Figure 4b). This value is normalized by the thickness (~10 μm) of the respective coating because there is a minor variation in thickness across samples, and this normalized intensity is written with the units of [intensity]/[length] or px/μm. In our recent publication, for all PS-*b*-PDMS species, a nonmonotonic behavior was seen—there was a short, rapid increase, followed by a peak formation at time $t = t_{peak}$, and then a slower decrease to a steady-state value.[42] We hypothesized that a similar nonmonotonic behavior in the penetration of PS-*b*-PVMS block copolymers seen here occurred through two concurrent directional penetration processes termed P1 and P2 (Figure 4a), which are governed by the thin geometry of the coating and not by an inherent material property (noting that we are only visualizing a small region in our imaging window, represented as a yellow box in Figure 4a). The faster process P1, which occurs along the micrometer-scale thickness of the coating in the vertical direction, is responsible for the rapid influx and accumulation of the dye, causing an increase in fluorescence intensity. Process P2 is along the lateral direction and transports the dye radially (over millimetric length scales) from underneath the drop to the "cleaner" regions of the coating with a lower dye concentration, decreasing the fluorescence intensity. Both P1 and P2 penetrations are driven by the difference in the chemical potential of the dye from high-concentration areas to low-concentration areas. For the PS-*b*-PVMS species, the fluorescence intensity continued to increase until 11 s, with a maximum fluorescence intensity of 3400 px/μm, and then continued to decrease within ~200 s, and its fluorescence intensity remained constant at around 2100 px/μm (Figure 4b). The fluorescence intensity over time shows that the penetration behavior of dye in all of the coatings can be generally divided into three regimes: (i) initially when process P1 (accumulation of the dye into the coating within our viewing window) dominates over P2 (diffusion of the dye toward cleaner regions outside our confocal microscope viewing window); (ii) around the local maxima; and (iii) a decay region where process P2 dominates over P1, resulting in a decrease of the fluorescence intensity until a balance in chemical potential difference creates a steady state at long time scales. For regime (i), when the dye drop has been just placed on the coating, the visualized penetration is dominated by the downward direction (P1); hence, the slope of intensity changes in the early stages of the experiment, long before the peak occurs ($d[\text{fluorescence intensity}]/dt$, $t \ll t_{peak}$), could be considered as a rate of penetration. As seen in Figure 4b,c, the values of $d[\text{fluorescence intensity}]/dt$ at $t \ll t_{peak}$ decrease with the length of fluorinated alkyl chains, which implies that the fluorination restricts the penetration of the dye into the coating and longer fluorinated alkyl chains should lead to a longer breakthrough time and better antipenetration.

For fluorinated species PS-*b*-P(CF_3-VMS), PS-*b*-P(n-C_2F_5-VMS), and PS-*b*-P(n-C_3F_7-VMS), the local maxima were observed at times 137, 378, and 732 s, respectively. This indicates that it takes a progressively longer time to attain the local maxima of fluorescence intensity as it becomes more

https://doi.org/10.1021/acsami.4c01905
ACS Appl. Mater. Interfaces XXXX, XXX, XXX−XXX

difficult for dyes to penetrate through the coatings with longer fluorinated alkyl chains. Also, these intensity maxima become lower with longer fluorinated alkyl chains. These two observations imply that both the rate and extent of dye penetration are restricted with increasing fluorination. For coatings of PS-*b*-P(*n*-C_4F_9-VMS) and PS-*b*-P(*n*-C_6F_{11}-VMS), only the initial period of increasing intensity is observed within the experiment time (Figure 4b, inset), and no local maxima are observed. This indicates that the penetration of the dye was limited in these polymers.

It should be noted that even though the average fluorescence intensity values of PS-*b*-PVMS are comparable to those of PS-*b*-P(*n*-C_6F_{13}-VMS), the extent and rate of penetration of these species are expected to be quite different. For the non-fluorinated PS-*b*-PVMS copolymer, the local maximum occurs within the first few seconds, leading to reduced accumulation inside the region that is visualized by confocal microscopy as it quickly moves toward cleaner regions of the coating away from the viewing window. This leads to lower measured intensity values. On the other hand, for the heavily fluorinated PS-*b*-P(*n*-C_6F_{11}-VMS) copolymer, the lack of a local maximum within the experimental time frame indicates a hindered influx of dye, again leading to low values of fluorescence intensity; in this instance, the dye is still making its way vertically into the coating within our viewing window. Hence, the PS-*b*-P(*n*-C_6F_{13}-VMS) coating, having the highest amount of fluorination, shows the best anti-penetration performance against the dye.

CONCLUSIONS

PDMS polymer has been widely used in surface coatings, but its high flexibility and mobility cause penetration problems of small molecules, which are not conducive to the stability of its chemical and physical properties. In this paper, fluorinated alkyl chains (*n*-$C_xF_{2x+1}(CH_2)_2$, x = 1−4 and 6) were grafted to the PS-*b*-PVMS backbone by thiol−ene click reactions. The introduction of fluorinated alkyl chains not only improves the hydrophobicity of the polymer, which can suppress surface wetting of water, but also causes inter-/intrachain interactions by silicon and fluorine atoms as electron donors and acceptors, respectively, which would limit the backbone flexibility and the mobility. At the same time, the rigidity of the fluorinated alkyl chains and the noted inter-/intrachain interactions would promote phase segregation or ordering of fluorinated side chains, which may cause tight-packing layers of fluorinated side chains to form. The improved hydrophobicity, limited flexibility of the backbone and mobility, and phase segregation of ordered fluorinated side chains work together to enhance the anti-penetration performance of PS-*b*-PVMS, as indicated by the in situ fluorescence tracking of Rhodamine B from an aqueous solution. More importantly, such antipenetration can be gradually improved with the length of the fluorinated alkyl chain, which may be further utilized to screen molecules of different sizes.

EXPERIMENTAL SECTION

Materials. *n*-$C_3F_7(CH_2)_2I$, *n*-$C_6F_{13}(CH_2)_2I$, anhydrous $MgSO_4$, and NaOH were purchased from Oakwood Products, Inc. *n*-$CF_3(CH_2)_2I$, *n*-$C_2F_5(CH_2)_2I$, and MeOH were purchased from VWR International. *sec*-Butyllithium solution (*sec*-BuLi, 1.4 M in cyclohexane), 2,2-dimethoxy-2-phenyl-acetophenone (DMPA), $(CH_3)_3SiCl$, CaH_2, thiourea, styrene, sodium, and benzene were purchased from Sigma-Aldrich. The providers of the following chemicals can be found in parentheses: EtOH (Decon Laboratories), HCl (aqueous solution with a concentration of 25% in volume, LabChem), tetrahydrofuran (THF, Avantor performance materials, US), hexamethylcyclotri-siloxane (D_3, BeanTown Chemical), and 1,3,5-trivinyl-1,3,5-trimethylcyclotrisiloxane (V_3, Chem Impex International). All of the above chemicals were used directly unless further processes were indicated.

Synthesis of Fluorinated Alkyl Thiols (*n*-$C_xF_{2x+1}(CH_2)_2SH$, x = 1−4, 6). The fluorinated alkyl thiols were synthesized according to a reported method (see Scheme 1).[68] A general method for thiol synthesis: a pear-shaped Schlenk flask of 50 mL with a magnetic stir bar was charged with ethanol (15 mL), *n*-$C_xF_{2x+1}(CH_2)_2SH$ (30 mmol, 1 equiv), and thiourea (1.5 equiv). The mixture was degassed by the freeze−pump−thaw method with N_2 as the inert gas. Then, the mixture was heated to reflux for 5 h and cooled to 50 °C. Degassed NaOH (1.2 equiv) and H_2O (11.6 equiv) were added to the flask, which was heated at 85 °C for 1 h. The reaction mixture was cooled to room temperature (R.T.), and degassed hydrochloric acid (1 M) was added excessively to acidify the mixture. Two immiscible liquids were found in the flask, and the bottom organic layer was transferred into a 2-dram vial by a pipet, which was washed with deionized water (1 mL) twice and dried with anhydrous $MgSO_4$. Then, the organic layer was distilled under the protection of N_2 to provide a purified target thiol in yields of 19−57%. The NMR spectra of synthesized fluorinated alkyl thiols are shown in Figures S2−S5 and 2a,b.

n-$CF_3(CH_2)_2SH$. ^{1}H NMR (400 MHz, $CDCl_3$) δ 2.72 (q, J = 8.1 Hz, 2H), 2.51−2.35 (m, 2H), 1.60 (t, J = 8.3 Hz, 1H). ^{19}F NMR (376 MHz, $CDCl_3$) δ −67.39 (t, J = 10.3, 10.3 Hz, 3F). Yield: 22%.

n-$C_2F_5(CH_2)_2SH$. ^{1}H NMR (400 MHz, $CDCl_3$) δ 2.76 (q, J = 8.3 Hz, 2H), 2.47−2.30 (m, 2H), 1.61 (t, J = 8.4 Hz, 1H).^{19}F NMR (376 MHz, $CDCl_3$) δ −86.41 (s, 3F), −119.26 (t, J = 17.5, 17.5 Hz, 2F). Yield: 53%.

n-$C_3F_7(CH_2)_2SH$. ^{1}H NMR (400 MHz, $CDCl_3$) δ = 2.83−2.70 (m, 2H), 2.51−2.33 (m, 2H), 1.61 (t, J = 8.4 Hz, 1H). ^{19}F NMR (376 MHz, $CDCl_3$) δ −81.52 (t, J = 9.6, 9.6 Hz, 3F), −116.21 − −116.41 (m, 2F), −128.73 − −128.84 (m, 2F). Yield: 34%.

n-$C_4F_9(CH_2)_2SH$. ^{1}H NMR (400 MHz, $CDCl_3$) δ = 2.83−2.72 (m, 2H), 2.52−2.34 (m, 2H), 1.61 (t, J = 8.4 Hz, 1H). ^{19}F NMR (376 MHz, $CDCl_3$) δ −81.96 − −82.03 (m, 3F), −115.46 − −115.63 (m, 2F), −125.43 − −125.47 (m, 2F), −126.94 − −127.05 (m, 2F). Yield: 19%.

n-$C_6F_{13}(CH_2)_2SH$. ^{1}H NMR (400 MHz, $CDCl_3$) δ 2.78 (q, J = 8.3 Hz, 2H), 2.52−2.34 (m, 2H), 1.61 (t, J = 8.4 Hz, 1H). ^{19}F NMR (376 MHz, $CDCl_3$) δ −81.72 − −81.79 (m, 3F), −115.21 − −115.42 (m, 2F), −122.79 − −122.93 (m, 2F), −123.73 − −123.86 (m, 2F), −124.45 − −124.55 (m, 2F), and −127.00 − −127.17 (m, 2F). Yield: 57%.

Synthesis of PS-*b*-PVMS. The synthesis of PS-*b*-PVMS was carried out by a reported anionic polymerization (see Scheme 1).[69] All reflux and distillation of solvents and reagents were under the protection of a superclean gas of N_2 or Ar. Both solvents of benzene and THF were dried by overnight reflux with CaH_2, distilled into another flask with Na, and further refluxed overnight. Styrene and V_3 were distilled under a vacuum after stirring with CaH_2 for a day. D_3 was dissolved in purified benzene and stirred with CaH_2 for a day, and then, it was distilled into a flask containing a living polystyrene-based anion, further stirred for a day, and then distilled under a vacuum. A Schlenk flask (50 mL) with a magnetic stirring bar was dried using a heat gun under vacuum and the protection of Ar. Then, 40 mL of THF and 0.21 mL of cyclohexane solution of *sec*-BuLi (1.4 M, 0.29 mmol) were stirred in a cold bath of acetone and dry ice (−78 °C) for 1 h. Styrene (2 mL, 17.46 mmol) was added to the reaction mixture and stirred for 1 h. Then, 0.5 mL of the sample was taken out and quenched in 5 mL of degassed MeOH (with a small amount of HCl) for the NMR and gel permeation chromatography (GPC) tests of the polystyrene block (PS). A benzene solution of D3 (1.22 M, 0.34 mmol) was added to the reaction mixture and stirred for 4 h. The cool bath was removed, and the reaction mixture was stirred for another hour at room temperature. Then, 0.4 mL of the sample was quenched by the same method as mentioned above for the NMR and GPC tests

https://doi.org/10.1021/acsami.4c01905
ACS Appl. Mater. Interfaces XXXX, XXX, XXX−XXX

of PS-D3. V3 (18.82 mmol) was added to the reaction mixture and stirred for 4 h, and 0.3 mL of trimethylchlorosilane was added and stirred overnight for termination. The product was purified by precipitation/dissolution three times with MeOH/THF. The structure of PS-*b*-PVMS was characterized by the NMR and GPC. The structure information based on the NMR and GPC tests of PS, PS-D3, and PS-*b*-PDMS can be seen in Table S1 and Figure S1.

Synthesis of PS-*b*-P(*n*-C_xF_{2x+1}-VMS). The thiol−ene click reaction between *n*-$C_xF_{2x+1}(CH_2)_2SH$ and PS-*b*-PVMS was carried out as shown in Scheme 1. A 40 mL vial was charged with 10 mL of THF solution of DMPA (69 mg) and PS-*b*-PVMS (710 mg, 3×10^{-5} mol). Another 40 mL vial was charged with 10 mL of THF solution of *n*-$C_xF_{2x+1}(CH_2)_2SH$ (8.2×10^{-3} mol) and a magnetic stirring bar. The two THF solutions were bubbled with N_2 or Ar for 15 min. The THF solution of *n*-$C_xF_{2x+1}(CH_2)_2SH$ was stirred under UV irradiation by slowly adding the THF solution of DMPA and PS-*b*-PVMS using a syringe pump in 30 min. The click reaction was carried out under UV irradiation for another 1 h. Then, PS-*b*-P(*n*-C_xF_{2x+1}-VMS) polymers were purified by methanol/THF (nonsolvent/solvent) and then dried in a vacuum oven with yields between 88 and 92%. PS-*b*-(*n*-C_xF_{2x+1}-PVMS) structures were characterized by ^{1}H, ^{19}F, and ^{29}Si NMR spectra (see Figures 2 and S2−S6 in the Supporting Information).

Characterization. ^{1}H, ^{19}F, and ^{29}Si NMR spectra were recorded by Bruker AV400 and AV500 with the peaks of $CHCl_3$, trifluorotoluene, and tetramethylsilane (TMS) as the reference, respectively. GPC tests were carried out on an Agilent 1200 system with a column set of PSS SDV for a separation range between 100 and 700 000 Da (Part number 201-0005) and a differential refractive index detector. The eluent was HPLC-grade THF, with 1% volume toluene as the internal standard, and the flow rate was 1 mL/min. The calibration of GPC tests was based on standard polymers of PS. DSC thermograms were measured by a TA Instruments DSC Auto 2500 with a temperature range between −90 and 150 °C by a heat−cool−heat program with heating and cooling rates of 10 °C.

THF solutions of PS-*b*-P(*n*-C_xF_{2x+1}-VMS) polymers (35 μL, 0.4 mg/μL) were cast into stainless steel flat washers (inner diameter of 5.3 mm, outer diameter of 10 mm, thickness of 1 mm). After 42 h, the solvent was evaporated, and the films of PS-*b*-P(*n*-C_xF_{2x+1}-VMS) polymers were obtained, which were put in an oven for thermal annealing at 120 °C for 61 h and then used for SAXS measurements. The SAXS measurements were carried out at the Functional Materials Beamline (FMB) of the Materials Solutions Network at the Cornell High Energy Synchrotron Source (MSN-C). An X-ray beam energy of 9.7 keV (λ = 1.28 Å) was selected using the 111 reflection of a single-bounce, HPHT diamond monochromator.[70] Harmonic rejection and vertical focusing are provided by a 1 m long, bendable, rhodium-coated monochromatic mirror located approximately 7 m upstream of the experimental hutch at an incident angle of 4 milliradians. Experiments were carried out in "bulk-beam" mode, and the monochromatic mirror was used to focus the beam into a spot approximately 0.08×0.5 mm^2 at the sample position, with a total flux of approximately 109 photons/s at 100 mA beam current.[70] Scattering images were collected on a Pilatus 300 K detector (Dectris, Baden, Switzerland) with a sample-to-detector distance of about 232 cm and equipped with a diode beamstop. Detector images were azimuthally integrated to produce intensity versus scattering vector, q(Å^{-1}), over a q-range of approximately 0.004−0.12 Å^{-1}. Plots were then corrected for both the incidence beam flux and sample absorption.

Water contact angle measurements were carried out via an Attension Theta Lite goniometer. THF solutions of PS-*b*-(*n*-C_xF_{2x+1}-PVMS) (1% in weight) were spin-coated on hexamethyldisilane-pretreated substrates (1.5×1.5 cm^2) of a silicon wafer with a setting of acceleration of 2500 rpm/s, speed of 5000 rpm, and spin time of 60 s. The coated slides were put in an oven (120−130 °C) for 24 h for thermal annealing. Three replicate-coated substrates of each polymer were obtained. Water contact angles of three points on each coated substrate were measured by dropping 10 μL of deionized water on the surfaces, and an average water contact angle of each PS-*b*-(*n*-C_xF_{2x+1}-PVMS)-coated surface was obtained.

Penetration Experiments. Details of the penetration tests and image analysis are described in a recent publication.[42] Briefly, the substrates used for the coatings were glass coverslips of thickness ∼0.15 mm that were cleaned using soap solution, distilled water, and ethanol, dried, and then placed in a UV−Ozone chamber for surface treatment. PS-*b*-P(*n*-C_xF_{2x+1}-VMS) was thoroughly dissolved in THF (30% by weight) and spin-coated onto the treated glass coverslips such that the film thickness was approximately 10 μm. This thickness was chosen for clarity in confocal microscopy imaging and to minimize aberration.

The coated substrate was loaded onto a Leica SP8 confocal microscope equipped with a piezo controller, and the *xz*-plane was viewed through a 40× objective, such that the cross-section of the coating was visible, along with both its interfaces with the air and glass (Figure 4a). A 20 μL drop of Rhodamine B in water of concentration 40 μg/g was placed on the focused region, and the confocal images were recorded at 2 frames/s. The experiments were curtailed at ∼15 min due to evaporation effects in the drop.

The images obtained were analyzed using MATLAB to obtain the change in the intensity of fluorescent dye inside the coating in both time and space. By integrating the intensity over the horizontal direction of the sample, we were able to calculate the variation in fluorescence inside the coating over time, which is represented as a 3D surface plot (Figure 4d−i). This allowed us to visualize how the dye localizes inside the coating over time. Further integration of this surface along the *z*-axis gives us the total intensity of the dye inside the coating at every point in time, which can be represented as a line graph (Figure 4b). This enables a comparison of penetration between different PS-*b*-P (*n*-C_xF_{2x+1}-VMS) coating species. Despite our best efforts to control it, the sample thicknesses vary slightly between samples. Hence, the intensity values are normalized by the thickness; thus, all fluorescence data have units of [intensity]/[length], represented as px/μm.

■ ASSOCIATED CONTENT

Supporting Information

The Supporting Information is available free of charge at https://pubs.acs.org/doi/10.1021/acsami.4c01905.

Molecular weight, dispersity ($Đ$), and degree of polymerization (DP) for the polymers involved in the anionic polymerization (Table S1); the GPC traces and NMR spectra of the polymers obtained in the synthesis of PS-*b*-PVMS (Figure S1); ^{1}H and ^{19}F NMR spectra for *n*-$C_xF_{2x+1}(CH_2)_2SH$, PS-*b*-PVMS, and PS-*b*-P(*n*-C_xF_{2x+1}-VMS) (x = 1−4 and 6, Figures S2−S5); ^{19}Si NMR spectra for PS-*b*-PVMS and PS-*b*-P(*n*-C_xF_{2x+1}-VMS) (Figure S6); and the flowability of the THF solutions of PS-*b*-P(*n*-C_xF_{2x+1}-VMS) (Figure S7) (PDF)

■ AUTHOR INFORMATION

Corresponding Author

Christopher K. Ober − *Department of Materials Science and Engineering, Cornell University, Ithaca, New York 14853, United States;* orcid.org/0000-0002-3805-3314; Email: cko3@cornell.edu

Authors

Zhenglin Zhang − *Department of Materials Science and Engineering, Cornell University, Ithaca, New York 14853, United States;* orcid.org/0000-0001-6740-5828

Krishnaroop Chaudhuri − *Department of Chemical and Environmental Engineering, University of Cincinnati, Cincinnati, Ohio 45221, United States;* orcid.org/0000-0003-4529-5351

https://doi.org/10.1021/acsami.4c01905
ACS Appl. Mater. Interfaces XXXX, XXX, XXX−XXX

Florian Kaefer − *Department of Materials Science and Engineering, Cornell University, Ithaca, New York 14853, United States;* orcid.org/0000-0003-4988-3812

Anthony P. Malanoski − *United States Naval Research Laboratory, Center for Biomolecular Science and Engineering, Washington, District of Columbia 20375, United States;* orcid.org/0000-0001-6192-888X

Kirt A. Page − *Cornell High Energy Synchrotron Source (CHESS), Cornell University, Ithaca, New York 14853, United States; Materials and Manufacturing Directorate, Air Force Research Laboratory, WPAFB, Dayton, Ohio 45433, United States; UES Inc., Dayton, Ohio 45432, United States;* orcid.org/0009-0000-7835-7657

Louisa M. Smieska − *Cornell High Energy Synchrotron Source (CHESS), Cornell University, Ithaca, New York 14853, United States;* orcid.org/0000-0001-8150-1920

Jonathan T. Pham − *Department of Chemical and Environmental Engineering, University of Cincinnati, Cincinnati, Ohio 45221, United States;* orcid.org/0000-0002-3433-8427

Complete contact information is available at: https://pubs.acs.org/10.1021/acsami.4c01905

Notes

The authors declare no competing financial interest.

■ ACKNOWLEDGMENTS

This research is primarily supported by the Defense Threat Reduction Agency (DTRA), contract number RD-CBT PS1BR-CB10828, via NRL contracts N00173-22-2-C001, N00173-22-2-C003, and N0017323C2019. This material is based on research sponsored by AFRL under agreement number FA8650-22-2-5200. The U.S. Government is authorized to reproduce and distribute reprints for Governmental purposes notwithstanding any copyright notation thereon. This work was performed in part at the Cornell NanoScale Facility, a member of the National Nanotechnology Coordinated Infrastructure (NNCI), which is supported by the National Science Foundation (Grant NNCI-2025233). The authors acknowledge the use of facilities and instrumentation supported by NSF through the Cornell MRSEC, the Cornell Center for Materials Research DMR-1719875. This work made use of the Cornell University NMR Facility, which is supported, in part, by the NSF through MRI award CHE-1531632. This work was also supported in part by funding provided by the Cornell Energy Systems Institute, Cornell University.

■ REFERENCES

(1) Ammar, S.; Ramesh, K.; Vengadaesvaran, B.; Ramesh, S.; Arof, A. K. Amelioration of Anticorrosion and Hydrophobic Properties of Epoxy/PDMS Composite Coatings Containing Nano ZnO Particles. *Prog. Org. Coat.* **2016**, *92*, 54−65.

(2) Amrutkar, S.; More, A.; Mestry, S.; Mhaske, S. T. Recent Developments in the Anti-Graffiti Coatings: an Attentive Review. *J. Coat. Technol. Res.* **2022**, *19*, 717−739.

(3) An, A. K.; Guo, J.; Lee, E.; Jeong, S.; Zhao, Y.; Wang, Z.; Leiknes, T. PDMS/PVDF Hybrid Electrospun Membrane with Superhydrophobic Property and Drop Impact Dynamics for Dyeing Wastewater Treatment Using Membrane Distillation. *J. Membr. Sci.* **2017**, *525*, 57−67.

(4) Sandru, M.; Sandru, E. M.; Ingram, W. F.; Deng, J.; Stenstad, P. M.; Deng, L.; Spontak, R. J. An Integrated Materials Approach to Ultrapermeable and Ultraselective CO2 Polymer Membranes. *Science* **2022**, *376*, 90−94.

(5) Leonardi, A. K.; Ober, C. K. Polymer-Based Marine Antifouling and Fouling Release Surfaces: Strategies for Synthesis and Modification. *Annu. Rev. Chem. Biomol. Eng.* **2019**, *10*, 241−264.

(6) Cao, Y.; Chen, X.; Matarasso, A.; Wang, Z.; Song, Y.; Wu, G.; Zhang, X.; Sun, H.; Wang, X.; Bruchas, M. R.; Li, Y.; Zhang, Y. Covalently Attached Slippery Surface Coatings to Reduce Protein Adsorptions on Poly(dimethylsiloxane) Planar Surfaces and 3D Microfluidic Channels. *ACS Appl. Mater. Interfaces* **2023**, *15*, 9987−9995.

(7) Lahiri, S. K.; Dijvejin, Z. A.; Golovin, K. Polydimethylsiloxane-Coated Textiles with Minimized Microplastic Pollution. *Nat. Sustainability* **2023**, *6*, 559−567.

(8) Teisala, H.; Baumli, P.; Weber, S. A. L.; Vollmer, D.; Butt, H.-J. Grafting Silicone at Room Temperature—a Transparent, Scratch-Resistant Nonstick Molecular Coating. *Langmuir* **2020**, *36* (16), 4416−4431.

(9) Rabnawaz, M.; Liu, G.; Hu, H. Fluorine-Free Anti-Smudge Polyurethane Coatings. *Angew. Chem., Int. Ed.* **2015**, *54*, 12722−12727.

(10) Zheng, W.; Huang, J.; Zang, X.; Xu, X.; Cai, W.; Lin, Z.; Lai, Y. Judicious Design and Rapid Manufacturing of a Flexible, Mechanically Resistant Liquid-Like Coating with Strong Bonding and Antifouling Abilities. *Adv. Mater.* **2022**, *34*, No. 2204581.

(11) Zhong, X.; Hu, H.; Yang, L.; Sheng, J.; Fu, H. Robust Hyperbranched Polyester-Based Anti-Smudge Coatings for Self-Cleaning, Anti-Graffiti, and Chemical Shielding. *ACS Appl. Mater. Interfaces* **2019**, *11*, 14305−14312.

(12) Colas, A. *Silicones: Preparation, Properties and Performance, Form No. 01−3077−01; Dow Corning* 2005.

(13) Wang, L.; McCarthy, T. J. Covalently Attached Liquids: Instant Omniphobic Surfaces with Unprecedented Repellency. *Angew. Chem., Int. Ed.* **2016**, *55*, 244−248.

(14) Huang, W.; Yang, J.; Zhang, C.; Zhou, W.; Li, Z.; Zhang, G.; Wang, L. Durable and Versatile Liquid-like Surfaces via the Base-Triggered Synthesis of Polysiloxane. *ACS Appl. Polym. Mater.* **2023**, *5*, 4578−4587.

(15) Liu, J.; Sun, Y.; Zhou, X.; Li, X.; Kappl, M.; Steffen, W.; Butt, H.-J. One-Step Synthesis of a Durable and Liquid-Repellent Poly(dimethylsiloxane) Coating. *Adv. Mater.* **2021**, *33*, No. 2100237.

(16) Wang, Y.; Yan, W.; Frey, M.; del Blanco, M. V.; Schubert, M.; Adobes-Vidal, M.; Cabane, E. Liquid-Like SiO_2-*g*-PDMS Coatings on Wood Surfaces with Underwater Durability, Antifouling, Antismudge, and Self-Healing Properties. *Adv. Sustainable Syst.* **2019**, *3*, No. 1800070.

(17) Shim, J.-u.; Cristobal, G.; Link, D. R.; Thorsen, T.; Jia, Y.; Piattelli, K.; Fraden, S. Control and Measurement of the Phase Behavior of Aqueous Solutions Using Microfluidics. *J. Am. Chem. Soc.* **2007**, *129*, 8825−8835.

(18) Randall, G. C.; Doyle, P. S. Permeation-driven Flow in Poly(dimethylsiloxane) Microfluidic Devices. *Proc. Natl. Acad. Sci. U.S.A.* **2005**, *102*, 10813−10818.

(19) Javaid, A. Membranes for Solubility-based Gas Separation Applications. *Chem. Eng. J.* **2005**, *112*, 219−226.

(20) Seethapathy, S.; Górecki, T. Applications of Polydimethylsiloxane in Analytical Chemistry: A Review. *Anal. Chim. Acta* **2012**, *750*, 48−62.

(21) Rumens, C. V.; Ziai, M. A.; Belsey, K. E.; Batchelor, J. C.; Holder, S. J. Swelling of PDMS Networks in Solvent Vapours; Applications for Passive RFID Wireless Sensors. *J. Mater. Chem. C* **2015**, *3*, 10091−10098.

(22) Belsey, K. E.; Parry, A. V.; Rumens, C. V.; Ziai, M. A.; Yeates, S. G.; Batchelor, J. C.; Holder, S. J. Switchable Disposable Passive RFID Vapour Sensors from Inkjet Printed Electronic Components Integrated with PDMS as a Stimulus Responsive. *J. Mater. Chem. C* **2017**, *5*, 3167−3175.

(23) Dangla, R.; Gallaire, F.; Baroud, C. N. Microchannel Deformations Due to Solvent-induced PDMS Swelling. *Lab Chip* **2010**, *10*, 2972−2978.
(24) Lee, J. N.; Park, C.; Whitesides, G. M. Solvent Compatibility of Poly(dimethylsiloxane)-Based Microfluidic Devices. *Anal. Chem.* **2003**, *75*, 6544−6554.
(25) Cai, Z.; Skabeev, A.; Morozova, S.; Pham, J. T. Fluid Separation and Network Deformation in Wetting of Soft and Swollen Surfaces. *Commun. Mater.* **2021**, *2*, 21.
(26) Spitzer, A. R.; Hutchens, S. B. Deformation-dependent Polydimethylsiloxane Permeability Measured Using Osmotic Microactuators. *Soft Matter* **2023**, *19*, 6005−6017.
(27) Hauer, L.; Cai, Z.; Skabeev, A.; Vollmer, D.; Pham, J. T. Phase Separation in Wetting Ridges of Sliding Drops on Soft and Swollen Surfaces. *Phys. Rev. Lett.* **2023**, *130*, No. 058205.
(28) Cai, Z.; Pham, J. T. How Swelling, Cross-Linking, and Aging Affect Drop Pinning on Lubricant-Infused, Low Modulus Elastomers. *ACS Appl. Polym. Mater.* **2022**, *4*, 3013−3022.
(29) Cheng, D. F.; Urata, C.; Yagihashi, M.; Hozumi, A. A Statically Oleophilic but Dynamically Oleophobic Smooth Nonperfluorinated Surface. *Angew. Chem., Int. Ed.* **2012**, *51*, 2956−2959.
(30) Chen, L.; Huang, S.; Ras, R. H.; Tian, X. Omniphobic Liquid-like Surfaces. *Nat. Rev. Chem.* **2023**, *7*, 123−137.
(31) Lamberti, A.; Marassoab, S. L.; Cocuzza, M. PDMS Membranes with Tunable Gas Permeability for Microfluidic Applications. *RSC Adv.* **2014**, *4*, 61415−61419.
(32) Sun, X.; Pan, Y.; Shen, C.; Zuo, C.; Ding, X.; Liu, G.; Xing, W.; Jin, W. Pollution and Cleaning of PDMS Pervaporation Membranes after Recovering Ethyl Acetate from Aqueous Saline Solutions. *Membranes* **2022**, *12*, 404.
(33) Oyama, T. G.; Oyama, K.; Taguchi, M. A Simple Method for Production of Hydrophilic, Rigid, and Sterilized Multi-layer 3D Integrated Polydimethylsiloxane Microfluidic Chips. *Lab Chip* **2020**, *20*, 2354−2363.
(34) Beaupre, D. M.; Goroncy, A. K.; Weiss, R. G. Influence of Concentration of Thiol-Substituted Poly(dimethylsiloxane)s on the Properties, Phases, and Swelling Behaviors of Their Crosslinked Disulfides. *Macromol* **2023**, *3*, 36−53.
(35) Cesaria, M.; Arima, V.; Manera, G. M.; Rella, R. Protocol of Thermal Aging against the Swelling of Poly(dimethylsiloxane) and Physical Insight in Swelling Regimes. *Polymer* **2018**, *139*, 145−154.
(36) Jeong, J.-M.; Oh, M. S.; Kim, B. J.; Choi, C.; Lee, B.; Lee, C.; Im, S. G. Reliable Synthesis of Monodisperse Microparticles: Prevention of Oxygen Diffusion and Organic Solvents Using Conformal Polymeric Coating onto Poly(dimethylsiloxane) Micromold. *Langmuir* **2013**, *29*, 3474−3481.
(37) Lee, J.; Kim, M. J.; Lee, H. H. Surface Modification of Poly(dimethylsiloxane) for Retarding Swelling in Organic Solvents. *Langmuir* **2006**, *22*, 2090−2095.
(38) Kim, B.; Hong, L.; Chung, Y.; Kim, D.; Lee, C. Solvent-Resistant PDMS Microfluidic Devices with Hybrid Inorganic/Organic Polymer Coatings. *Adv. Funct. Mater.* **2009**, *19*, 3796−3803.
(39) Hong, T.; Chatterjee, S.; Mahurin, S. M.; Fan, F.; Tian, Z.; Jiang, D.; Long, B. K.; Mays, J. W.; Sokolov, A. P.; Saito, T. Impact of Tuning CO_2-Philicity in Polydimethylsiloxane-Based Membranes for Carbon Dioxide Separation. *J. Membr. Sci.* **2017**, *530*, 213−219.
(40) Hong, T.; Cao, P.; Zhao, S.; Li, B.; Smith, C.; Lehmann, M.; Erwin, A. J.; Mahurin, S. M.; Venna, S. R.; Sokolov, A. P.; Saito, T. Tailored CO_2-philic Gas Separation Membranes via One-pot Thiolene Chemistry. *Macromolecules* **2019**, *52*, 5819−5828.
(41) Barry, M. E.; Davidson, E. C.; Zhang, C.; Patterson, A. L.; Yu, B.; Leonardi, A. K.; Duzen, N.; Malaviya, K.; Clarke, J. L.; Finlay, J. A.; Clare, A. S.; Chen, Z.; Ober, C. K.; Segalman, R. A. The Role of Hydrogen Bonding in Peptoid-Based Marine Antifouling Coatings. *Macromolecules* **2019**, *52*, 1287−1295.
(42) Chaudhuri, K.; Medhi, R.; Zhang, Z.; Cai, Z.; Ober, C. K.; Pham, J. T. Visualizing Penetration of Fluorescent Dye through Polymer Coatings. *Macromol. Rapid Commun.* **2023**, *44*, No. 2300304.
(43) Sato, Y.; Hayami, R.; Gunji, T. Characterization of NMR, IR, and Raman spectra for siloxanes and silsesquioxanes: a mini review. *J. Sol−Gel Sci. Technol.* **2022**, *104*, 36−52.
(44) Kim, S.-Y.; Saxena, A.; Kwak, A.; Fujiki, M.; Kawakami, Y. Cooperative C-F···Si Interaction in Optically Active Helical Polysilanes. *Chem. Commun.* **2004**, 538−539.
(45) Kawabe, T.; Naito, M.; Fujiki, M. Polysilane Organogel with Hierarchical Structures Formed by Weak Intra-/Inter-chain Si/FC and van der Waals Interactions. *Polym. J.* **2008**, *40*, 317−326.
(46) Chu, J. H.; Rangarajan, P.; Adams, J. L.; Register, R. A. Morphologies of Strongly Segregated Polystyrene-poly(dimethylsiloxane) Diblock Copolymers. *Polymer* **1995**, *36*, 1569−1575.
(47) Liontos, G.; Manesi, G.; Moutsios, I.; Moschovas, D.; Piryazev, A. A.; Bersenev, E. A.; Ivanov, D. A.; Avgeropoulos, A. Synthesis, Molecular Characterization, and Phase Behavior of Miktoarm Star Copolymers of the AB_n and A_nB (n = 2 or 3) Sequences, Where A Is Polystyrene and B Is Poly(dimethylsiloxane). *Macromolecules* **2022**, *55*, 88−99.
(48) Petr, M.; Hammond, P. T. Room Temperature Rapid Photoresponsive Azobenzene Side Chain Liquid Crystal Polymer. *Macromolecules* **2011**, *44*, 8880−8885.
(49) Mabry, J. M.; Vij, A.; Iacono, S. T.; Viers, B. D. Fluorinated Polyhedral Oligomeric Silsesquioxanes (F-POSS). *Angew. Chem., Int. Ed.* **2008**, *47*, 4137−4140.
(50) Rim, P. B.; Rasoul, H. A. A.; Hurley, S. M.; Orler, E. B.; Scholsky, K. M. Rheological and thermal properties of poly(methylalkylsiloxane). *Macromolecules* **1987**, *20*, 208−211.
(51) Wang, J.; Mao, G.; Ober, C. K.; Kramer, E. J. Liquid Crystalline, Semifluorinated Side Group Block Copolymers with Stable Low Energy Surfaces: Synthesis, Liquid Crystalline Structure, and Critical Surface Tension. *Macromolecules* **1997**, *30*, 1906−1914.
(52) Wang, J.; Ober, C. K. Solid State Crystalline and Liquid Crystalline Structure of Semifluorinated 1-Bromoalkane Compounds. *Liq. Cryst.* **1999**, *26*, 637−648.
(53) Shen, Q.; Interrante, L. V. Synthesis, Characterization, and Glass Transitions of Some Asymmetrically Substituted Poly(siloxanes). *Macromolecules* **1997**, *30*, 5485−5489.
(54) Ninago, M. D.; Satti, A. J.; Ciolino, A. E.; Vallés, E. M.; Villar, M. A.; Vega, D. A.; Sanz, A.; Nogales, A.; Rueda, D. R. Synthesis and Morphology of Model PS-*b*-PDMS Copolymers. *J. Polym. Sci., Part A: Polym. Chem.* **2010**, *48*, 3119−3127.
(55) Li, T.; Wang, Z.; Schulte, L.; Hansen, O.; Ndoni, S. Fast & Scalable Pattern Transfer via Block Copolymer Nanolithography. *RSC Adv.* **2015**, *5*, 102619−102624.
(56) Arias-Zapata, J.; Böhme, S.; Garnier, J.; Girardot, C.; Legrain, A.; Zelsmann, M. Ultrafast Assembly of PS-PDMS Block Copolymers on 300 mm Wafers by Blending with Plasticizers. *Adv. Funct. Mater.* **2016**, *26*, 5690−5700.
(57) Georgopanos, P.; Lo, T.; Ho, R.; Avgeropoulos, A. Synthesis, molecular characterization and self-assembly of $(PS\text{-}b\text{-}PDMS)_n$ type linear (n = 1, 2) and star (n = 3, 4) block copolymers. *Polym. Chem.* **2017**, *8*, 843−850.
(58) Manesi, G.-M.; Chang, C.; Avgeropoulos, A.; Ho, R. Interdomain Spacing Control via an Interdigitating Structure to Bilayers in Lamellae-Forming Star-Block Copolymers. *ACS Appl. Polym. Mater.* **2020**, *2*, 3685−3695.
(59) Cong, W.; Gao, W.; Garvey, C. J.; Dumée, L. F.; Zhang, J.; Kent, B.; Wang, G.; She, F.; Kong, L. In Situ SAXS Measurement and Molecular Dynamics Simulation of Magnetic Alignment of Hexagonal LLC Nanostructures. *Membranes* **2018**, *8*, 123.
(60) Lai, C.; Russel, W. B.; Register, R. A. Phase Behavior of Styrene−Isoprene Diblock Copolymers in Strongly Selective Solvents. *Macromolecules* **2002**, *35*, 841−849.
(61) Lee, K.; Kreider, M.; Bai, W.; Cheng, L.; Dinachali, S. S.; Tu, K.; Huang, T.; Ntetsikas, K.; Liontos, G.; Avgeropoulos, A.; Ross, C. A. UV-solvent Annealing of PDMS-majority and PS-majority PS-b-PDMS Block Copolymer Films. *Nanotechnology* **2016**, *27*, No. 465301.

https://doi.org/10.1021/acsami.4c01905
ACS Appl. Mater. Interfaces XXXX, XXX, XXX−XXX

(62) Chang, C.-Y.; Manesi, G.-M.; Avgeropoulos, A.; Ho, R.-M. Superlattice Structure from Self-Assembly of High-χ Block Copolymers via Chain Interdigitation. *Macromolecules* **2022**, *55*, 3449−3457.
(63) Leung, S. C. E.; Wanninayake, D.; Chen, D.; Nguyen, N.; Li, Q. Physicochemical properties and interactions of perfluoroalkyl substances (PFAS)—Challenges and opportunities in sensing and remediation. *Sci. Total Environ.* **2023**, *905*, No. 166764.
(64) Wang, Z.; Pujari, S. P.; van Lagen, B.; Smulders, M. M. J.; Zuilhof, H. Highly Polymer-Repellent yet Atomically Flat Surfaces Based on Organic Monolayers with a Single Fluorine Atom. *Adv. Mater. Interfaces* **2016**, *3*, No. 1500514.
(65) Graupe, M.; Takenaga, M.; Koini, T.; Colorado, R.; Lee, T. R. Oriented Surface Dipoles Strongly Influence Interfacial Wettabilities. *J. Am. Chem. Soc.* **1999**, *121*, 3222−3223.
(66) Colorado, R.; Lee, T. R. Wettabilities of Self-Assembled Monolayers on Gold Generated from Progressively Fluorinated Alkanethiols. *Langmuir* **2003**, *19*, 3288−3296.
(67) Yu, T.; Marquez, M. D.; Zenasni, O.; Lee, T. R. Mimicking Polymer Surfaces Using Cyclohexyl- and Perfluorocyclohexyl-Terminated Self-Assembled Monolayers. *ACS Appl. Nano Mater.* **2019**, *2*, 5809−5816.
(68) Behr, F. E.; Dams, R. J.; DeWitte, J. E.; Hagen, D. F. Perfluoroalkyl Halides and Derivatives. US6,048,952A, 2000.
(69) Petr, M.; Katzman, B.-A.; DiNatale, W.; Hammond, P. T. Synthesis of a New, Low-T_g Siloxane Thermoplastic Elastomer with a Functionalizable Backbone and Its Use as a Rapid, Room Temperature Photoactuator. *Macromolecules* **2013**, *46*, 2823−2832.
(70) Stoupin, S.; Krawczyk, T.; Sagan, D.; Temnykh, A.; Smieska, L.; Woll, A.; Ruff, J.; Lyndaker, A.; Pauling, A.; Croom, B. P.; Trigg, E. B. Side-bounce beamlines using single-reflection diamond monochromators at Cornell High Energy Synchrotron Source. *J. Synchrotron Radiat.* **2021**, *28*, 429−438.

https://doi.org/10.1021/acsami.4c01905
ACS Appl. Mater. Interfaces XXXX, XXX, XXX−XXX